Nanotechnology

PAPER • OPEN ACCESS

Growth behavior during metalorganic chemical vapor deposition of MoS_2 using di-tert-butyl sulfide as organic sulfur precursor

To cite this article: J H (Sanne) Deijkers *et al* 2026 *Nanotechnology* **37** 035601

View the article online for updates and enhancements.

You may also like

- Influence of growth temperature on MoS_2 synthesis by chemical vapor deposition
Zusong Zhu, Shengbao Zhan, Jie Zhang et al.

- Controllable growth of monolayer MoS_2 by chemical vapor deposition via close MoO_2 precursor for electrical and optical applications
Yong Xie, Zhan Wang, Yongjie Zhan et al.

- Influence of chemical potential on shape evolution of 2D-MoS_2 flakes produced by chemical vapor deposition
Mula Raju, Meher Wan, Supriti Sen et al.

This content was downloaded from IP address 146.103.254.11 on 23/04/2026 at 10:09

Nanotechnology

OPEN ACCESS

RECEIVED
16 July 2025

REVISED
9 December 2025

ACCEPTED FOR PUBLICATION
17 December 2025

PUBLISHED
16 January 2026

Original content from this work may be used under the terms of the Creative Commons Attribution 4.0 licence.

Any further distribution of this work must maintain attribution to the author(s) and the title of the work, journal citation and DOI.

PAPER

Growth behavior during metalorganic chemical vapor deposition of MoS_2 using di-tert-butyl sulfide as organic sulfur precursor

J H (Sanne) Deijkers[1,2,*], H Medina Silva[2], A Manasi[2,3,4], S Pasko[4], W M M (Erwin) Kessels[1], A J M Mackus[1], B Groven[2] and A Delabie[2,3,*]

[1] Department of Applied Physics and Science Education, Eindhoven University of Technology, Eindhoven, The Netherlands
[2] imec, Kapeldreef 75, Leuven 3001, Belgium
[3] Department of Chemistry, KU Leuven (University of Leuven), B-3001 Leuven, Belgium
[4] AIXTRON SE, Dornkaulstr. 2, Herzogenrath 52134, Germany
[*] Author to whom any correspondence should be addressed.

E-mail: j.h.deijkers@tue.nl and Annelies.Delabie@imec.be

Keywords: synthesis, MoS_2, di-tert-butyl sulfide, metalorganic chemical vapor deposition, growth behavior, 2D transition metal chalcogenide

Supplementary material for this article is available online

Abstract

Metalorganic chemical vapor deposition is a promising synthesis technique for two-dimensional materials such as MoS_2. In this study, we controlled the growth mode of MoS_2 on SiO_2 using $Mo(CO)_6$ and di-tert-butyl sulfide as precursors by adjusting the process conditions. The growth was directed from amorphous deposition at 400 °C and 500 °C, to crystalline MoS_2 at 600 °C and higher. From 750 °C, not only MoS_2 grains were deposited, but Mo metal nuclei were also formed during the process. An enhancement of the grain size was achieved by increasing the S/Mo precursor ratio. A more effective method to enlarge the grains and to lower the number density of crystals was to anneal the SiO_2 substrate in Ar atmosphere prior to deposition. The reduced number density suggested that the pretreatment increased the diffusion length of Mo adatom species on the surface. Furthermore, addition of H_2 to the N_2 carrier gas had two effects on the growth mode, without altering the amount of deposited Mo. On one hand, due to a higher fraction of H_2 in the carrier gas, the grain size slightly increased, and on the other hand, a change towards Mo metal deposition was observed. Control of the process conditions offers the opportunity to deposit large MoS_2 grains without co-depositing Mo metal.

1. Introduction

Since the isolation of a single layer of graphene in 2004 [1], two-dimensional (2D) materials have attracted considerable attention [2–4]. Transition metal dichalcogenides (TMDs) are a class of 2D materials consisting of a transition metal atom sandwiched between chalcogen atoms. The class of TMDs is diverse, ranging from semiconducting to metallic materials. Specifically, MoS_2 is an interesting TMD as it is a semiconducting material. Multilayer MoS_2 has an indirect band gap, which transitions to an direct band gap at the monolayer level [5]. MoS_2 can, for instance, be applied in field-effect transistors (FETs), photodetectors, catalysts, and Cu diffusion barriers [6–9]. For the key application as the channel material in FETs, the single monolayer of 6.15 Å thick is the most interesting in terms of properties, due to the high mobility at low thicknesses. Therefore, it is crucial to achieve the synthesis of high-quality monolayers in order to replace Si channels with MoS_2 channels. Different synthesis options include mechanical exfoliation, liquid exfoliation, sulfurization of molybdenum oxides, (metalorganic) chemical vapor deposition ((MO)CVD), atomic layer deposition (ALD), and molecular beam epitaxy [10, 11]. Indirect, transfer-based, methods (e.g. exfoliation) are not suitable for commercial fabrication, while direct approaches (e.g. vapor phase synthesis techniques) allow for large-area growth [12].

© 2026 The Author(s). Published by IOP Publishing Ltd

Metalorganic chemical vapor deposition (MOCVD) involves a metalorganic precursor, which enables deposition at lower temperatures than CVD using other metal precursors, such as metal halide molecules. Moreover, MOCVD provides control over film composition, and results in high-quality materials with, for instance, large crystal grain sizes. Therefore, MOCVD is a promising technique for high-quality deposition of TMDs on the wafer scale [13, 14]. In addition to the metal precursor, various chalcogen precursors have been studied. H_2S is a frequently used S precursor, although organic S precursors are becoming a more popular option, especially in the academia, to avoid costly facilities measures, such as toxic detection systems, related to the toxicity of H_2S [15]. Moreover, organic S precursors can more easily be obtained commercially in high purity (e.g. electronic grade 5N). Another advantage is that they are typically liquids and can be used in easy-to-operate bubblers. A disadvantage of using an organic S precursor is the possible formation of C impurities during deposition, which can be incorporated in the TMD film, or form a carbonaceous layer on the interface. The use of an organic S precursor is believed to result in films with a similar quality as compared with H_2S [16].

2D TMDs synthesized by MOCVD employing an organic S precursor form films of high quality with large grains [8, 17], minimal bilayer formation [18], and good conformality [19]. The films exhibit a high mobility [20], a high photoluminescence response [12], and good electrical properties [21]. C incorporation can be limited by either introducing H_2 [16], or by limiting the maximal deposition temperature to 700 °C [22]. In the different studies about 2D TMD film growth by MOCVD using various precursors and reactor setups, several factors have been determined that affect the growth behavior. A higher process temperature leads to a decrease in crystal density with a corresponding increase in grain size [12, 13, 18, 21, 23, 24]. The effect of changing the chalcogen to metal precursor ratio was investigated in several studies. For the growth of MoS_2 on SiO_2 by $Mo(CO)_6$ and H_2S, as well as for the growth of WSe_2 on sapphire by $W(CO)_6$ and diisopropyl selenide, no significant change in the nucleation or grain size was observed [25, 26]. On the other hand, WSe_2 grown on sapphire by $W(CO)_6$ and dimethyl selenide showed more multilayer growth and larger grains when the Se/W precursor ratio was increased [27]. Furthermore, when the diethyl sulfide to $Mo(CO)_6$ ratio was increased for MoS_2 grown on SiO_2, the grains changed shape and more C was incorporated [16]. Additionally, lowering the S/W precursor ratio led to W metal growth in MOCVD of WS_2 on SiO_2 using $W(CO)_6$ and di-tert-butyl sulfide (DTBS) [21]. For the impact of a pretreatment of a SiO_2 surface, it was found that a prebake in first N_2, and then in S atmosphere, resulted in a reduction of the nucleation density [21]. H_2 addition to the carrier gas was shown to enhance precursor decomposition and limit C incorporation [8, 13, 19, 21], while it also led to etching of the 2D TMD film, thus resulting in smaller grains or a lower growth rate [16, 20]. Besides the choice of carrier gas, the combination of a high carrier gas flow rate and a high pressure resulted in a low nucleation density [25].

In this work, we investigated the MOCVD growth behavior of MoS_2 on SiO_2 using $Mo(CO)_6$ as Mo precursor and DTBS ($((CH_3)_3C)_2S$) as S precursor, in order to expand the understanding of the growth mechanisms. With respect to earlier studies involving DTBS, the difference is the combination of the direct deposition on SiO_2 in a shower head reactor and the studies on the impact of the process parameters, namely the $Mo(CO)_6$ to DTBS ratio, an Ar pretreatment, and H_2 addition to a N_2 carrier gas. The effect of process temperature on the deposition was investigated by observing the effect on the nucleation and growth. Besides an effect on the MoS_2 grain size, Mo metal nucleation was observed at high temperatures. Several S/Mo precursor ratios were tested, and a higher S/Mo ratio resulted in a lower number density of crystals and larger grains, which has been attributed to a larger diffusion length. Pretreatment of the SiO_2 surface in Ar atmosphere was found to also increase the grain size, to a larger extent than the increase in S/Mo precursor ratio. Finally, addition of H_2 to the N_2 carrier gas was studied, which led to more Mo metal deposition, while the growth rate was unaffected.

2. Experimental methods

MoS_2 was deposited by MOCVD in an AIXTRON 300 mm MOCVD Close Coupled Showerhead reactor in 200 mm configuration for the growth of 2D materials, of which a schematic is shown in figure 1. All films were deposited on thermal SiO_2 on Si substrates using molybdenum hexacarbonyl ($Mo(CO)_6$) and DTBS as precursors for Mo and S respectively. The $Mo(CO)_6$ flow was $1.2 \cdot 10^{-7}$ mol min^{-1}, and the DTBS flow was varied from $5.1 \cdot 10^{-4}$ mol min^{-1} to $2.5 \cdot 10^{-3}$ mol min^{-1}. The growth process was performed under N_2/H_2 atmosphere, where the addition of H_2 is assumed to assist in precursor decomposition. The total flow was 18 slm, of which the H_2 flow rate was varied from 0 to 4 slm (0%–22%). A pressure of 50 mbar was used. Unless otherwise stated, the deposition temperature was 700 °C, and the H_2 addition was set at 11%. The substrates were either not pretreated prior to deposition, or annealed in Ar atmosphere at 900 °C for 5 min.

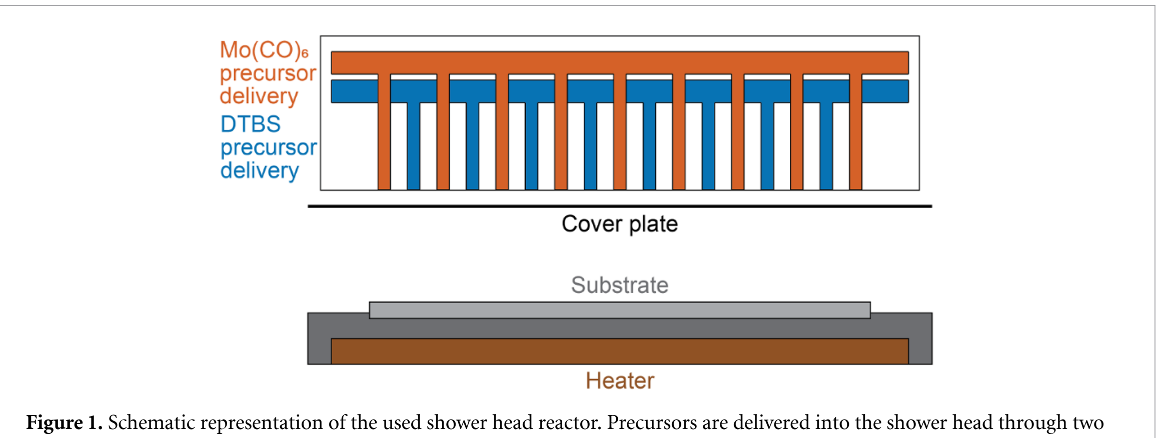

Figure 1. Schematic representation of the used shower head reactor. Precursors are delivered into the shower head through two separate inlets.

The samples were characterized by atomic force microscopy (AFM), scanning electron microscopy (SEM), Rutherford backscattering spectroscopy (RBS), x-ray photoelectron spectroscopy (XPS), Raman spectroscopy, and x-ray fluorenscence (XRF). A Dimension Icon instrument from Bruker was used to characterize the morphology of the deposited MoS_2 crystals by AFM. The AFM images were captured in PeakForce QNM mode using a Si tip (HQ-NSC19/AlBS). Later, data was processed in Gwyddion software. A FEI Verios tool with TLD-SE detector was used to capture SEM images. The used beam energy was between 1 and 2 keV, the beam current was 50–100 pA, and the working distance was 1–1.5 mm. From AFM and SEM images, we characterized the morphology of deposited MoS_2 crystals, and extracted crystal density, and crystal size distribution. Further analysis of the SEM images was performed to extract the number density of crystals. The StarDist plugin in ImageJ, as developed by Schmidt *et al*, was used to identify and count the number of nuclei on the surface [28]. To use the StarDist plugin in ImageJ, the colors of the SEM images were inverted. RBS was used to determine the Mo:S ratio and the thickness of the deposited MoS_2. A 1.523 MeV He^+ ion beam and a scatter angle of 170° was used. The XPS measurements were carried out in Angle Integrated mode using a QUANTES instrument from Physical electronics. The measurements were performed using a monochromatized photon beam of 1486.6 eV and a 100 μm spot. Charge neutralization was used during this experiment. The used substrates were 200 mm in diameter and measurements were performed on the center, the middle, and on the edge of the wafer. Since no significant differences were observed as a function of position, only the measurements on the center are presented.

3. Results and discussion

3.1. Simplified growth model

Combining insights from literature and based on the following results, we propose a simplified growth model of the different gas phase and surface reactions, which is schematically shown in figure 2. Both precursors, $Mo(CO)_6$ and DTBS, and the carrier gas consisting of N_2 and H_2, are flown through the reactor. The $Mo(CO)_6$ precursor decomposes in the gas phase, after which the Mo atoms adsorb on the surface [8, 16]. DTBS decomposes above 380 °C into H_2S and hydrocarbons such as isobutene [29, 30]. For simplicity, $Mo(CO)_6$ is assumed to decompose fully into Mo and CO, and for DTBS only H_2S and isobutene are considered as reaction products. H_2S is believed to act as the main sulfur source, while isobutene serves as a source for C co-deposition. At the surface H_2S decomposes further. Diffusion of Mo and S over the surface leads to the nucleation and growth of MoS_2. When the process temperature is increased, the residence time of S adatoms decreases. Mo is assumed to not desorb [31], thus, there is relatively more Mo on the surface at high temperatures, which stimulates Mo metal growth. H_2, which is present in the carrier gas, can etch S preferentially [32], also leading to Mo metal growth. Moreover, H_2 can limit C co-deposition, by etching the deposited C [8, 16].

3.2. Effect of temperature on growth

The process temperature determines the growth regime, which is either a mass transport limited or a reaction rate limited regime. The MOCVD process was executed at 400 °C–800 °C for 360 s, which corresponds to the early nucleation phase. For these depositions the substrate was pretreated in Ar atmosphere at 900 °C. The growth rate was measured by XRF and RBS, and the results are shown in

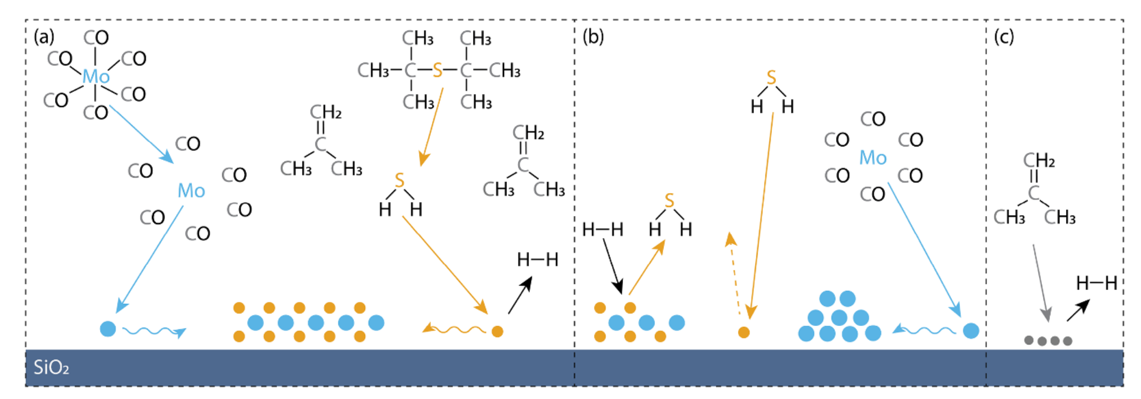

Figure 2. Schematic of different gas phase and surface processes during the MOCVD of MoS_2, (a) MoS_2 deposition, (b) Mo metal growth, and (c) C co-deposition. The $Mo(CO)_6$ precursor decomposes fully into Mo and CO, while the DTBS precursor decomposes into H_2S and isobutene. In the reaction of H_2S with the SiO_2 surface, H_2 is created when S species adsorb. The isobutene can result in C co-deposition upon the release of H_2.

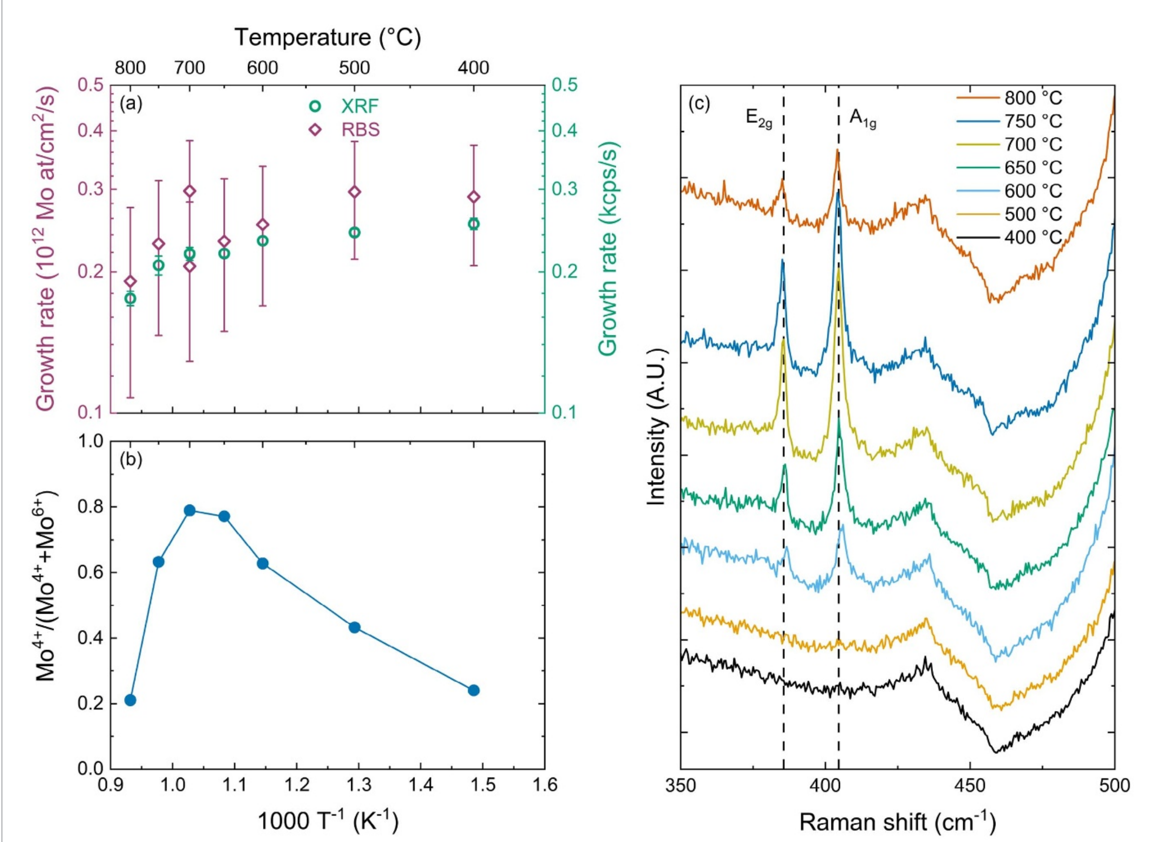

Figure 3. (a) Growth rate from the amount of Mo as measured by RBS and XRF as a function of process temperature. At 700 °C two individual samples were measured, demonstrating that there is a slight sample-to-sample variation. (b) Mo^{4+} oxidation state with respect to the total Mo^{4+} and Mo^{6+} in the film, as measured by *ex situ* XPS, as a function of process temperature. Mo^0 was not observed. (c) Raman spectra of films deposited at different temperatures, 400 °C–800 °C. The spectra were normalized to the Si peak and have a vertical offset for clarity. The characteristic peaks for crystalline 2H-MoS_2 are indicated.

figure 3(a). Due to the low coverage, the amount of S was lower than the detection limit for RBS, and could not be measured. While the growth rate remained constant between 400 °C and 500 °C, a slight decrease of the growth rate was observed for process temperatures above 500 °C. The observed decrease in growth rate at temperatures above ∼600 °C can be attributed to the premature thermal decomposition of the precursors used, primarily the rate-limiting $Mo(CO)_6$ precursor [33]. Therefore, it can be concluded that the growth is mass transport limited in the range from 400 °C to 800 °C.

While the amount of deposited Mo is fairly independent of the deposition temperature, the morphology and composition are temperature dependent, as indicated by AFM, XPS, and Raman analysis.

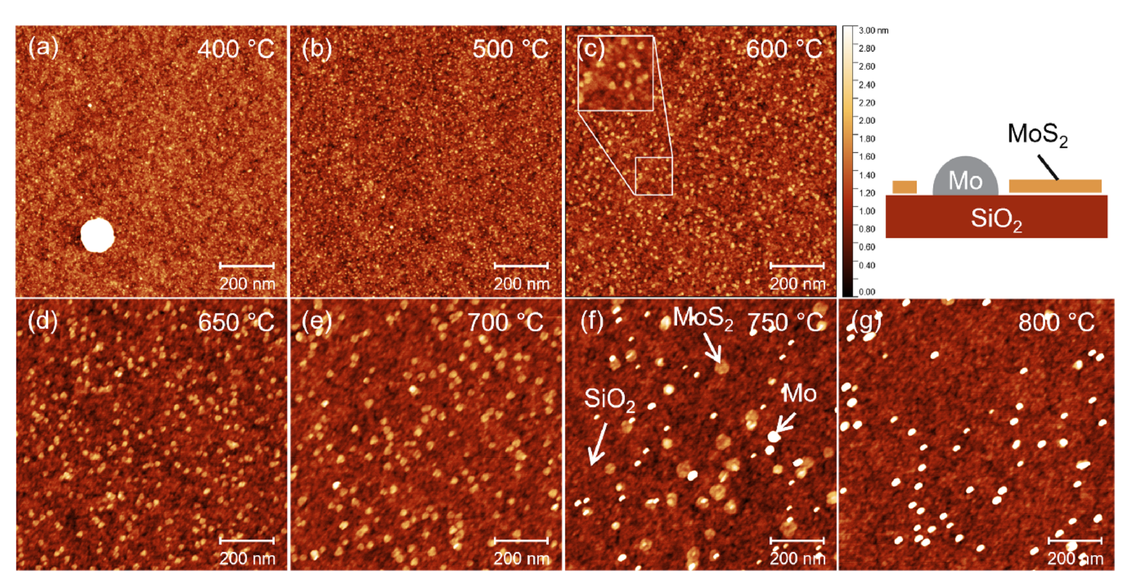

Figure 4. AFM images of films deposited at different temperatures, in the range of 400 °C–800 °C. For the process temperature of 400 °C the large circular particle is expected to be contamination due to exposure to the atmosphere. (c) The inset in the image for 600 °C shows a zoom in on the surface. (f) For the process temperature of 750 °C, deposited MoS_2 grains, deposited Mo metal nuclei, and the SiO_2 substrate are indicated. The cross-sectional schematic at the top right shows MoS_2 grains and a Mo metal nucleus on a SiO_2 surface.

Figure 4 shows the corresponding AFM images of the aforementioned data, the corresponding height distributions are shown in figure S1 in the supplementary information (SI). A temperature of 400 °C or 500 °C does not result in detectable MoS_2 grains in AFM, while from figure 3(a) it could be concluded that material is deposited. Possibly, an amorphous film was deposited at these temperatures. From 600 °C triangular MoS_2 grains are visible by AFM. The MoS_2 grain size increases when the temperature is increased and the grains become hexagonally shaped. The larger grains are due to a larger Mo adatom diffusion length because of the higher temperature. Furthermore, at 750 °C and 800 °C Mo metal nuclei are visible in addition to the MoS_2 grains. The Mo metal nuclei can be distinguished by the larger height and different shape compared the MoS_2 grains [34]. Mo metal nuclei are known to grow as 3D islands, while MoS_2 grains are expected to grow laterally as 2D crystals. At these high temperatures, fast desorption of S species leads to more Mo metal growth. At 750 °C multiple Mo metal nuclei are visible together with some MoS_2 grains on the surface, while at 800 °C and higher hardly any MoS_2 grains are detected. An additional morphological analysis, based on line profiles from AFM for a width of 100 nm is presented in figure S3 in the SI.

XPS measurements, which were performed after air exposure, show the presence of both Mo^{4+} and Mo^{6+} oxidation states, besides the expected Si and O peaks from the SiO_2 substrate. Sulfur was observed in the S^{2-} oxidation state, confirming the MoS_2 composition. Some of the Mo3d spectra are shown in figure S4 in the SI. Figure 3(b) shows the relative amounts of Mo in the 4+ and 6+ oxidation states. Below 600 °C, Mo is mostly in the Mo^{6+} oxidation state, which matches the hypothesis that at these temperatures an amorphous MoS_x film is deposited, with $x > 2$. Additionally, it is hypothesized that the amorphous MoS_x film is oxidized strongly during air exposure between deposition and the XPS measurement, as was seen for low-temperature ALD of WS_2 [35]. From 600 °C to 750 °C, Mo is mostly in the Mo^{4+} oxidation state, confirming the presence of MoS_2. At 800 °C, the 6+ oxidation state becomes dominant, which could be related to the presence of oxidized Mo metal nuclei on the surface, again due to air exposure between deposition and the XPS measurement. Mo^0 of Mo metal was not found in the Mo3d spectrum. Possibly, the small metal nuclei are oxidized at their surface, resulting in more Mo^{6+} than Mo^0.

The presence of crystalline MoS_2 at 600 °C and higher was confirmed by Raman spectroscopy measurements, see figure 3(c). Raman spectroscopy is typically used to assess the crystallinity and structural quality of 2D materials, in particular in-plane order [36]. For MoS_2, the E_{2g} and A_{1g} peaks are expected to be found for the crystalline 2H-MoS_2 phase [37]. The weak Raman signal is due to the low coverage of ∼10% of MoS_2 on the SiO_2 surface. The apparent baseline tilt is due to the presence of peaks corresponding to Si at 301 and 520 cm^{-1}, before the latter peak there is a small peak and

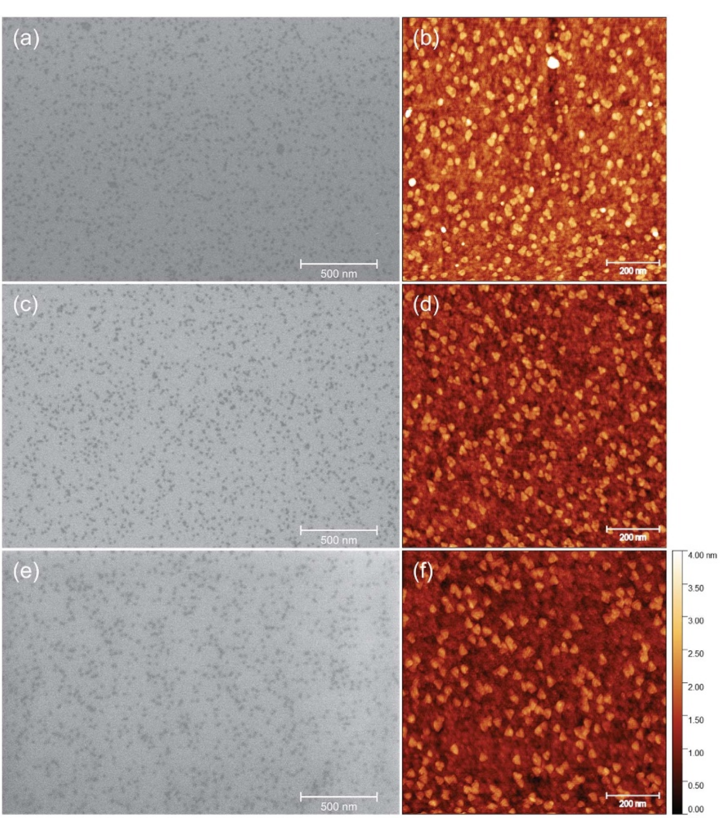

Figure 5. (a), (c), (e) SEM images and (b), (d), (f) AFM images of the SiO_2 surface (light gray in the SEM images) with MoS_2 grains (dark gray in the SEM images) for a growth time of 600 s. S/Mo precursor ratio of (a), (b) $4.4 \cdot 10^3$, (c), (d) $10.3 \cdot 10^3$, and (e), (f) $20.9 \cdot 10^3$. From the SEM images the number density of crystals is extracted (figure 6). Please note that the scales of the SEM and AFM images are different, the AFM images are a factor 1.7 more zoomed in.

valley located. For 400 °C and 500 °C no Raman response of MoS_2 is observed, indicative of either a lack of crystalline material, or such small crystals that they cannot be measured by Raman spectroscopy. For 600 °C and higher, the characteristic E_{2g} and A_{1g} peaks of 2H-MoS_2 are present, which is at a slightly higher temperature than expected for MOCVD. The locations of the E_{2g} and A_{1g} peaks are ∼386 and ∼405 cm^{-1}, respectively, and they do not change significantly as a function of temperature. From figure 3(a) a decrease in growth rate for increasing temperature was observed. Therefore, the increase in Raman intensity from 600 °C to 700 °C and from 700 °C to 750 °C can be attributed to the improved crystal quality. The decrease in Raman intensity at 800 °C was most likely caused by less MoS_2, since the AFM images in figure 4 show more Mo metal deposition, and a lack of MoS_2 grains.

3.3. Modulation of the nucleation behavior by DTBS/$Mo(CO)_6$ ratio and pretreatment

To study the effect of the DTBS/$Mo(CO)_6$ precursor ratio, MoS_2 films were grown using different DTBS flows, while keeping the $Mo(CO)_6$ flow constant. The constant $Mo(CO)_6$ flow in combination with a constant temperature of 700 °C ensures the same growth rate for the different precursor ratios, see figure S6 in the SI. The deposition was carried out for multiple growth times to study different moments in the early deposition stage before film closure. The crystallinity of the films was verified by Raman spectroscopy, as shown in figures S7 and S8 in the SI. The S/Mo precursor ratio was varied from $(4.4 \pm 0.1) \cdot 10^3$ to $(20.9 \pm 0.1) \cdot 10^3$. Increasing the chalcogen to metal precursor flow rate results in a lower nucleation density and larger grains as the amount of deposited material is similar [27]. This could suggest that surface diffusion of adspecies is promoted when the (surface) concentration of chalcogen atoms increases. SEM and AFM images after 600 s of MoS_2 growth using different S/Mo precursor ratios, shown in figure 5, confirm that a higher S/Mo precursor ratio results in a lower number density of crystals and larger grains.

In theory, as a function of growth time, the number density of crystals N increases initially due to the formation of new nuclei. Subsequently, N reaches a steady-state regime where existing crystals grow and no new crystals are formed. In this steady-state regime, the average distance between existing crystals provides a rough estimation of the diffusion length of the adspecies. Lastly, coalescence of

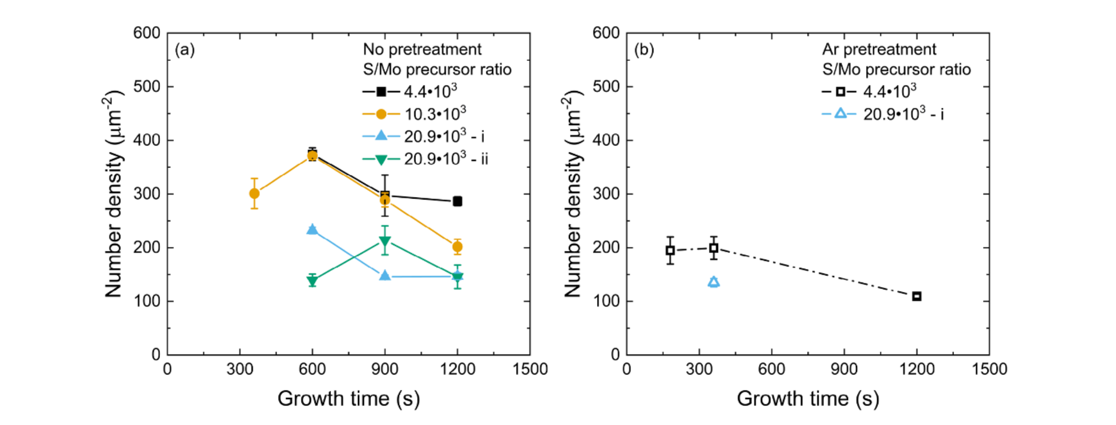

Figure 6. Number density of crystals of MoS_2 grains extracted from SEM images as function of growth time for different S/Mo precursor ratios. (a) No pretreatment and (b) Ar pretreatment. At the ratios of $20.9 \cdot 10^3$ two separate samples were measured, indicated by i and ii.

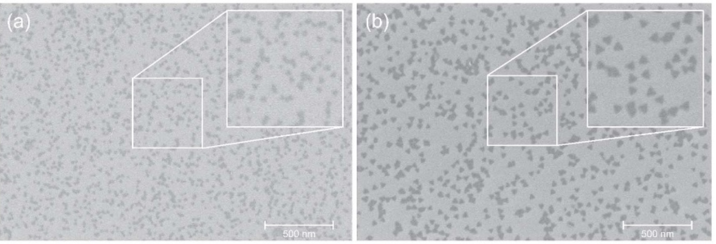

Figure 7. SEM images of MoS_2 grown for 1200 s with S/Mo precursor ratio of $4.4 \cdot 10^3$ on (a) SiO_2 without pretreatment, and (b) SiO_2 with a pretreatment consisting of a 300 s anneal at 900 °C in Ar atmosphere. The insets show a zoom in on the surface.

nuclei should result in a decrease in N. From multiple SEM images per S/Mo precursor ratio, the number density of crystals N was determined for MoS_2 as described in section 2. In figure 6, N of MoS_2 grains as a function of the growth time is shown for different S/Mo precursor ratios. The presented data in figure 6(a) shows that N decreases for longer growth times, confirming coalescence of grains. There is slight sample to sample variation, as can be seen by the two data sets at ratio $(20.9 \pm 0.1) \cdot 10^3$. Increasing the S/Mo precursor ratio from $(4.4 \pm 0.1) \cdot 10^3$ to $(10.3 \pm 0.1) \cdot 10^3$ leads to a sharper reduction of the number density of crystals for 1200 s of growth time. An even higher S/Mo precursor ratio of $(20.9 \pm 0.1) \cdot 10^3$ shows that per growth time the number density of crystals is reduced more than at the lower ratios. The slightly changing number density for times <1200 s suggests that the growth appears to be in a steady-state regime before coalescence, where the crystals grow mainly by diffusion-driven aggregation [38]. Therefore, it can be estimated that the diffusion length of the adspecies increases with increasing S/Mo precursor ratio, since the number density of crystals in this steady-state regime decreases.

Besides the S/Mo precursor ratio, the nucleation behavior is affected by the pretreatment of the SiO_2 surface. In figures 6(b) and 7, a difference can be seen between the resulting grain size and number density of crystals as a result of the pretreatment. An Ar anneal at 900 °C for 300 s leads to larger grains and a lower number density of crystals, while the total amount of deposited material remains the same, see figure S6 in the SI. An explanation for the lower number density of crystals is that the Ar pretreatment anneal reduces the number of hydroxyl groups, and thus lowers the number of available surface sites for nucleation of MoS_2 [39–41]. The extracted number density of crystals as presented in figure 6 of the pretreated samples at a ratio of $(4.4 \pm 0.1) \cdot 10^3$ is lower than that of the untreated samples for all measured growth times. The lower N and less coalescence for the pretreated samples makes it more straightforward to study the effect of S/Mo precursor ratio on the diffusion length. For untreated samples this is more challenging as there is relatively early coalescence.

3.4. Effect of H_2 co-dosing on the growth mode

Adding H_2 to the gas mixture during deposition is known to lead to fewer carbon impurities [8, 42], but can also result in smaller grains [20]. Furthermore, H_2 can induce preferential S etching, which would

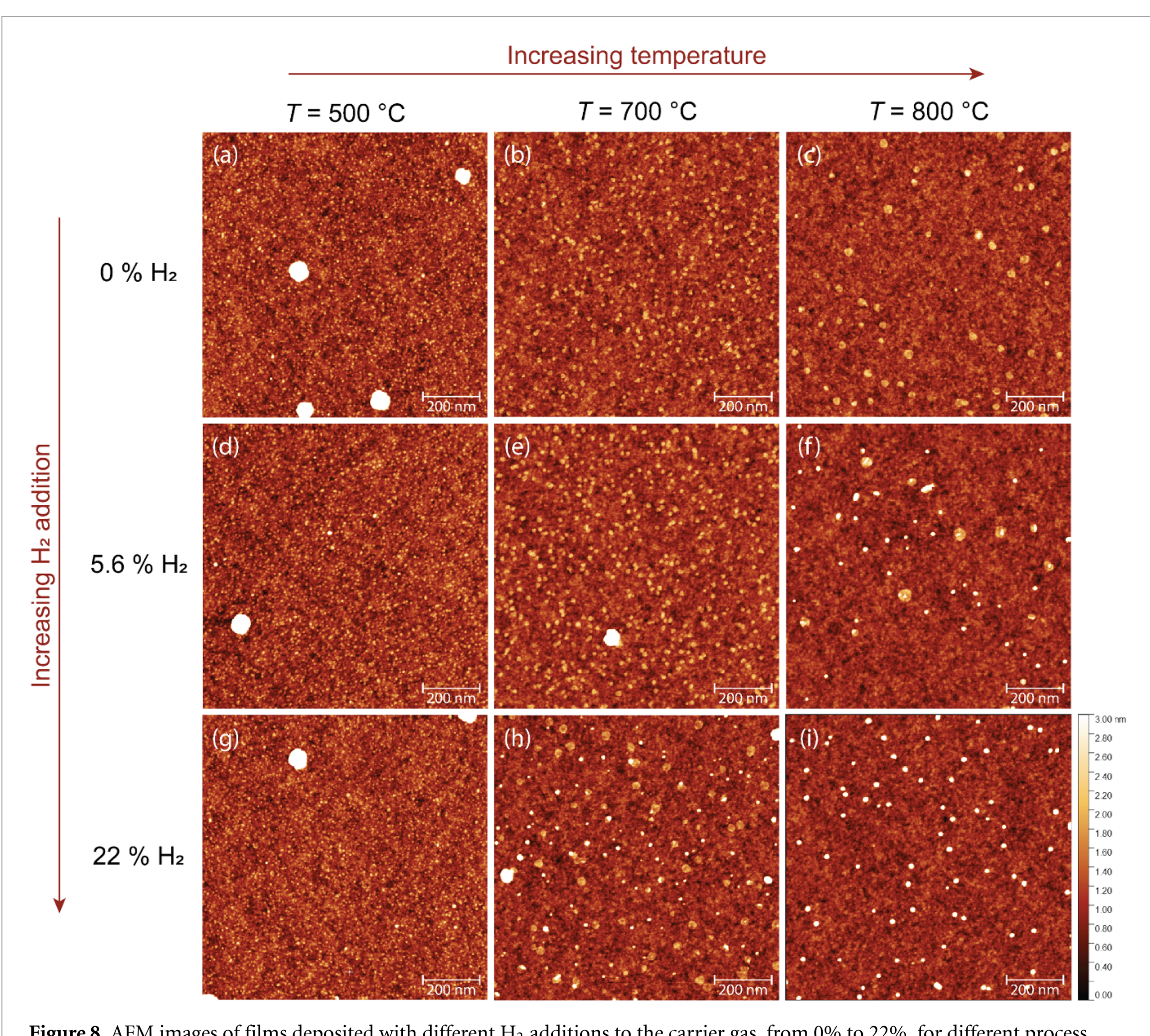

Figure 8. AFM images of films deposited with different H_2 additions to the carrier gas, from 0% to 22%, for different process temperatures, 500 °C, 700 °C, and 800 °C. The large spots on the surface at 500 °C are likely contamination particles.

produce less MoS_2 and more Mo metal growth. The effect of H_2 was investigated by varying the amount of added H_2 to the N_2 carrier gas, from 0% to 22% of the total flow. The total flow is kept constant at 18 slm. AFM images for different H_2 additions and temperatures are shown in figure 8, the corresponding height distributions are shown in figure S2 in the SI. Per H_2 flow rate the trend as a function of the temperature is similar. A higher temperature results in larger grains and possibly Mo metal nuclei growth, as was also seen in section 3.2. Per temperature the effect of H_2 can be distinguished. At 500 °C no MoS_2 grains are observed independent of the H_2 flow. Increasing the H_2 addition to the carrier gas for 700 °C and 800 °C on the other hand, leads to larger grains, hexagonally shaped grains, and more Mo metal nuclei formation. The change in grain shape and the formation of Mo metal nuclei are probably caused by etching of S by H_2. Adding H_2 leads to etching of S, which changes the shape of the grains and leads to more Mo metal growth, similar to the effect of increasing the process temperature. Therefore, either adding H_2 or increasing the temperature can be used to control the growth behavior.

Figure 9 shows the amount of Mo and S on the surface of the samples of figure 8 measured by XRF. The Mo amount does not change significantly per temperature even if more H_2 is added to the carrier gas. This shows that the temperature defines the growth rate. The S amount decreases for increasing H_2 flow at 700 °C and 800 °C, which supports the hypothesis of S etching by H_2. The decrease in S counts complements the observation that Mo metal is grown instead of MoS_2. From XPS (see figure S5 in the SI) at 800 °C a shift to higher binding energies is observed when more H_2 was added.

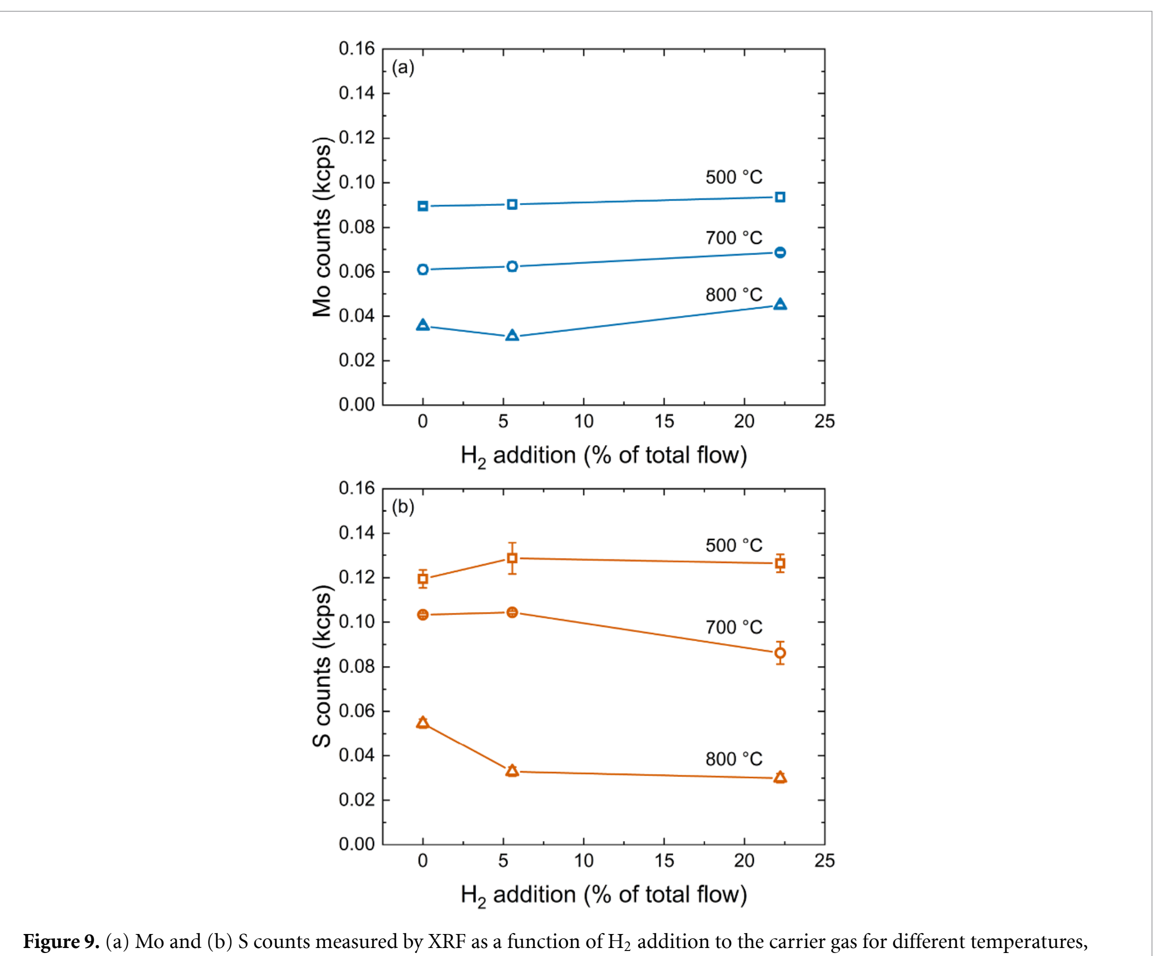

Figure 9. (a) Mo and (b) S counts measured by XRF as a function of H_2 addition to the carrier gas for different temperatures, 500 °C, 700 °C, and 800 °C.

4. Conclusions

In this work we studied the effect of different process conditions on the growth of MoS_2 by MOCVD using $Mo(CO)_6$ and DTBS. We found that the process temperature has an optimal range for crystalline MoS_2 without Mo metal, namely from 600 °C to 700 °C. Increasing the S/Mo precursor ratio results in larger grains and less nuclei. Enlarging the grains and reducing the number density of crystals can also be achieved by pretreating the SiO_2 substrate prior to deposition using an Ar anneal. The lower number density of crystals is most likely due to a longer diffusion length of the Mo adatom on the SiO_2 surface. Addition of H_2 to the N_2 carrier gas barely affects the amount of deposited Mo. However, the growth mode changes from predominantly MoS_2 grain growth to Mo metal growth when more H_2 is added. The change towards more Mo metal deposition was also seen for increasing the process temperature. This study provides new understanding of the growth of MoS_2 by MOCVD using $Mo(CO)_6$ and DTBS, where the MoS_2 grain size can be increased and Mo metal deposition can be prevented by controlling the process conditions.

Data availability statement

The data cannot be made publicly available upon publication due to legal restrictions preventing unrestricted public distribution. The data that support the findings of this study are available upon reasonable request from the authors.

Supplementary Information available at https://doi.org/10.1088/1361-6528/ae2e05/data1.

Acknowledgments

The authors kindly acknowledge the vital support from the imec lab and fab teams, the supply chain team, and the facility, process, and hardware engineering teams, the imec pilot line and the materials and components analysis teams. This work was performed in the imec Industrial Affiliation Program

(IIAP) core CMOS and received funding from the European Union's Graphene Flagship 2D-PL (Grant Agreement No. 101189797). We kindly acknowledge the measurements and analysis by RBS from Johan Meersschaut and Johan Desmet, by AFM from Stefanie Sergeant, Danielle Vanhaeren, and Inge Vaesen, XPS from Thierry Conard and by SEM from Ehsan Jazaeri, Hans Billington and Eva Grieten.

Conflicts of interest

The authors have no conflicts to disclose.

Author contributions

J H (Sanne) Deijkers 0000-0003-1762-4349
Conceptualization (lead), Data curation (lead), Formal analysis (lead), Investigation (lead), Methodology (lead), Visualization (lead), Writing – original draft (lead)

H Medina Silva 0000-0003-1461-5703
Conceptualization (equal), Data curation (equal), Formal analysis (equal), Investigation (equal), Methodology (equal), Supervision (equal), Writing – review & editing (equal)

A Manasi
Data curation (equal), Investigation (equal), Methodology (equal), Visualization (equal), Writing – review & editing (supporting)

S Pasko 0000-0001-6718-106X
Project administration (supporting), Resources (equal), Writing – review & editing (equal)

W M M (Erwin) Kessels 0000-0002-7630-8226
Supervision (supporting), Writing – review & editing (equal)

A J M Mackus 0000-0001-6944-9867
Conceptualization (supporting), Formal analysis (supporting), Project administration (equal), Supervision (supporting), Writing – review & editing (equal)

B Groven 0000-0002-5781-7594
Conceptualization (supporting), Formal analysis (supporting), Project administration (lead), Resources (equal), Supervision (equal), Writing – review & editing (equal)

A Delabie 0000-0001-9739-7419
Conceptualization (supporting), Formal analysis (supporting), Project administration (equal), Resources (equal), Supervision (equal), Writing – review & editing (equal)

References

[1] Novoselov K S, Geim A K, Morozov S V, Jiang D, Zhang Y, Dubonos S V, Grigorieva I V and Firsov A A 2004 Electric field effect in atomically thin carbon films *Science* **306** 666–9

[2] Das S, Robinson J A, Dubey M, Terrones H and Terrones M 2015 Beyond graphene: progress in novel two-dimensional materials and van der Waals solids *Annu. Rev. Mater. Res.* **45** 1–27

[3] Manzeli S, Ovchinnikov D, Pasquier D, Yazyev O V and Kis A 2017 2D transition metal dichalcogenides *Nature Rev. Mater.* **2** 17033

[4] Minghui Li, Lin Li, Fan Y, Jiao F, Geng D and Wenping H 2022 From top to down-recent advances in etching of 2D materials *Adv. Mater. Interfaces* **9** 2201334

[5] Ellis J K, Lucero M J and Scuseria G E 2011 The indirect to direct band gap transition in multilayered MoS_2 as predicted by screened hybrid density functional theory *Appl. Phys. Lett.* **99** 261908

[6] Mortelmans W *et al* 2024 Record performance in GAA 2D NMOS and PMOS using monolayer MoS_2 and WSe_2 with scaled contact and gate length *Digest of Technical Papers - Symp. on VLSI Technology* (Institute of Electrical and Electronics Engineers Inc.) (https://doi.org/10.1109/VLSITechnologyandCir46783.2024.10631395)

[7] Krishnan U, Kaur M, Singh K, Kumar M and Kumar A 2019 A synoptic review of MoS_2: synthesis to applications *Superlattices Microstruct.* **128** 274–97

[8] Mawlong L P L, Hoang A T, Chintalapalli J, Seunghyeon J, Lee K, Kim K and Ahn J H 2023 Reduced defect density in MOCVD-Grown MoS_2 by manipulating the precursor phase *ACS Appl. Mater. Interfaces* **15** 47359–67

[9] Deijkers J H, de Jong A A, Mattinen M J, Schulpen J J P M, Verheijen M A, Sprey H, Maes J W, Kessels W M M, Bol A A and Mackus A J M 2023 MoS_2 synthesized by atomic layer deposition as Cu diffusion barrier *Adv. Mater. Interfaces* **10** 2202426

[10] Alam S, Chowdhury M A, Shahid A, Alam R and Rahim A 2021 Synthesis of emerging two-dimensional (2D) materials—advances, challenges and prospects *FlatChem* **30** 11

[11] Joseph S, Mohan J, Lakshmy S, Thomas S, Chakraborty B, Thomas S and Kalarikkal N 2023 A review of the synthesis, properties and applications of 2D transition metal dichalcogenides and their heterostructures *Mater. Chem. Phys.* **297** 3

[12] Andrzejewski D, Marx M, Grundmann A, Pfingsten O, Kalisch H, Vescan A, Heuken M, Kümmell T and Bacher G 2018 Improved luminescence properties of MoS_2 monolayers grown via MOCVD: role of pre-treatment and growth parameters *Nanotechnology* **29** 295704

[13] Tang S, Grundmann A, Fiadziushkin H, Ghiami A, Heuken M, Vescan A and Kalisch H 2022 Detailed study on MOCVD of wafer-scale MoS_2 monolayers: from nucleation to coalescence *MRS Adv.* **7** 751–56

[14] Zhang X, Lai J and Gray T 2023 Recent progress in low-temperature CVD growth of 2D materials *Oxf. Open Mater. Sci.* **3** itad010

[15] Batterman S, Grant-Alfieri A and Seo S H 2023 Low level exposure to hydrogen sulfide: a review of emissions, community exposure, health effects and exposure guidelines *Crit. Rev. Toxicol.* **53** 244–95

[16] Schaefer C M, Caicedo Roque J M, Sauthier G, Bousquet J, Hébert C, Sperling J R, Pérez-Tomás A, Santiso J, Corro E D and Garrido J A 2021 Carbon incorporation in MOCVD of MoS_2 thin films grown from an organosulfide precursor *Chem. Mater.* **33** 4474–87

[17] Marx M, Grundmann A, Lin Y R, Andrzejewski D, Kümmell T, Bacher G, Heuken M, Kalisch H and Vescan A 2018 Metalorganic vapor-phase epitaxy growth parameters for two-dimensional MoS_2 *J. Electron. Mater.* **47** 910–6

[18] Tang S, Grundmann A, Fiadziushkin H, Wang Z, Hoffmann-Eifert S, Ghiami A, Debald A, Heuken M, Vescan A and Kalisch H 2023 Migration-enhanced metal-organic chemical vapor deposition of wafer-scale fully coalesced WS2 and WSe_2 monolayers *Cryst. Growth Des.* **23** 1547–58

[19] Cho K, Sawamoto N, Machida H, Ishikawa M, Sudoh H, Wakabayashi H, Yokogawa R and Ogura A 2023 Conformal deposition of WS_2 layered film by low-temperature metal-organic chemical vapor deposition *Jpn. J. Appl. Phys.* **62** SG1048

[20] Kang K, Xie S, Huang L, Han Y, Huang P Y, Mak K F, Kim C J, Muller D and Park J 2015 High-mobility three-atom-thick semiconducting films with wafer-scale homogeneity *Nature* **520** 656–60

[21] Wen Chia W, Huang K N, Chien Ying S, Kei C C, Kuo C H and Chien C H 2023 Wafer-scale MOCVD grown WS_2 with normally off transistor behavior and its general application on different amorphous substrates *Appl. Phys. Lett.* **123** 183101

[22] Tang H *et al* 2023 Nucleation and coalescence of tungsten disulfide layers grown by metalorganic chemical vapor deposition *J. Cryst. Growth* **608** 127111

[23] Cwik S, Mitoraj D, Reyes O M, Rogalla D, Peeters D, Kim J, Schütz H M, Bock C, Beranek R and Devi A 2018 Direct growth of MoS_2 and WS_2 layers by metal organic chemical vapor deposition *Adv. Mater. Interfaces* **5** 1–11

[24] Chen C *et al* 2024 Effect of growth temperature on the microstructure and properties of epitaxial MoS_2 monolayers grown by metalorganic chemical vapor deposition *J. Vac. Sci. Technol. A* **42** 022201

[25] Kim T, Mun J, Park H, Joung D, Diware M, Won C, Park J, Jeong S H and Kang S W 2017 Wafer-scale production of highly uniform two-dimensional MoS_2 by metal-organic chemical vapor deposition *Nanotechnology* **28** 18LT01

[26] Grundmann A *et al* 2023 Impact of synthesis temperature and precursor ratio on the crystal quality of MOCVD WSe_2 monolayers *Nanotechnology* **34** 205602

[27] Zhang X, Balushi Z Y A, Zhang F, Choudhury T H, Eichfeld S M, Alem N, Jackson T N, Robinson J A and Redwing J M 2016 Influence of carbon in metalorganic chemical vapor deposition of few-layer WSe_2 thin films *J. Electron. Mater.* **45** 6273–9

[28] Schmidt U, Weigert M, Broaddus C and Myers G 2018 Cell detection with star-convex polygons *Int. Conf. on Medical Image Computing and Computer-Assisted Intervention (MICCAI)* (*Granada, Spain*) (https://doi.org/10.1007/978-3-030-00934-2_30)

[29] Martin G and Barroeta N 1980 Gas phase thermolysis of sulfur compounds. II. Ditertiary butyl sulfide *Int. J. Chem. Kinet.* **12** 699–716

[30] Class C A, Liu M, Vandeputte A G and Green W H 2016 Automatic mechanism generation for pyrolysis of di-tert-butyl sulfide *Phys. Chem. Chem. Phys.* **18** 21651–8

[31] Yeh C C, Lai Y H, Chu W Y, Yeh C T and Hung W H 2004 Photon-induced chemical vapor deposition of molybdenum on Pt(111) *Surf. Sci.* **565** 81–88

[32] Shike H *et al* 2020 Detecting the repair of sulfur vacancies in CVD-grown MoS_2 domains via hydrogen etching *J. Electron. Mater.* **49** 2547–55

[33] Lewis K E, Golden D M and Smith G P 1984 Organometallic bond dissociation energies: laser pyrolysis of iron pentacarbonyl, chromium hexacarbonyl, molybdenum hexacarbonyl, and tungsten hexacarbonyl *J. Am. Chem. Soc.* **106** 3905–12

[34] Verdin J *et al* 2024 Process-induced modulation of domain orientations during WS2 epitaxy by metal-organic chemical vapor deposition on sapphire *ACS Appl. Electron. Mater.* **6** 6758–69

[35] Groven B *et al* 2017 Plasma-enhanced atomic layer deposition of two-dimensional WS_2 from WF_6, H_2 plasma and H_2S *Chem. Mater.* **29** 2927–38

[36] Cong X, Liu X L, Lin M L and Tan P H 2020 Application of Raman spectroscopy to probe fundamental properties of two-dimensional materials *npj 2D Mater. Appl.* **4** 1–12

[37] Hong Li, Zhang Q, Yap C C R, Tay B K, Edwin T H T, Olivier A and Baillargeat D 2012 From bulk to monolayer MoS_2: evolution of Raman scattering *Adv. Funct. Mater.* **22** 1385–90

[38] Zhang Z and Lagally M G 1997 Atomistic processes in the early stages of thin-film growth *Science* **276** 377–83

[39] Clerix J-W J, Dianat G, Delabie A and Parsons G N 2023 *In situ* analysis of nucleation reactions during $TiCl_4/H_2O$ atomic layer deposition on SiO_2 and H-terminated Si surfaces treated with a silane small molecule inhibitor *J. Vac. Sci. Technol. A* **41** 3

[40] Mun J, Kim Y, Kang I S, Lim S K, Lee S J, Kim J W, Park H M, Kim T and Kang S W 2016 Low-temperature growth of layered molybdenum disulphide with controlled clusters *Sci. Rep.* **6** 1–7

[41] Vandalon V and (Erwin) Kessels W M M 2017 Revisiting the growth mechanism of atomic layer deposition of Al_2O_3: a vibrational sum-frequency generation study *J. Vac. Sci. Technol. A* **35** 05C313

[42] Chiappe D *et al* 2018 Layer-controlled epitaxy of 2D semiconductors: bridging nanoscale phenomena to wafer-scale uniformity *Nanotechnology* **29** 425602